


Sertoli Cells Loaded with Doxorubicin in Lipid Micelles Reduced Tumor Burden and Dox-Induced Toxicity

Cell Transplantation
2017, Vol. 26(10) 1694-1702
© The Author(s) 2017
Reprints and permission:
sagepub.com/journalsPermissions.nav
DOI: 10.1177/0963689717721223
journals.sagepub.com/home/cil


Mahasweta Das^{1,2}, Mark Howell³, Elspeth A. Foran³, Rohit Iyres²,
Shyam S. Mohapatra^{1,2,4}, and Subhra Mohapatra^{1,3,4}

Abstract

The toxic side effects of doxorubicin (Dox) limit its long-term use as a lung cancer chemotherapeutic. Additionally, drug delivery to the deep lung is challenging. To address these challenges, isolated rat Sertoli cells (SCs) were preloaded with Dox conjugated to lipid micelle nanoparticles (SC-DLMNs) and delivered to mouse lungs. These immunocompetent cells, when injected intravenously, travel to the lung, deliver the payload, and get cleared by the system quickly without causing any adverse reaction. We observed that SC-DLMNs effectively treated Lewis lung carcinoma I-induced lung tumors in mice and the drug efficacy was comparable to SC-Dox treatment. Mice treated with SC-DLMNs also showed significantly less toxicity compared to those treated with SC-Dox. The encapsulation of Dox in lipid micelle nanoparticles reduced the toxicity of Dox and the SC-based delivery method ensured drug delivery to the deep lung without evoking any immune response. Taken together, these results provide a novel SC-based nanoparticle drug delivery method for improved therapeutic outcome of cardiotoxic antitumor cancer drugs.

Keywords

Sertoli cell, lung cancer, lipid micelle nanoparticles, drug toxicity, doxorubicin (Dox)

Introduction

Lung cancer is one of the leading causes of death in the western world.¹ Surgery, radiotherapy, chemotherapy, and immunotherapy remain the standard treatment options for lung cancers.² Despite several improvements in chemotherapeutic drug delivery systems, delivery of drugs to the lungs, especially to the deep lung, remains a major challenge. One of the main drug delivery routes to the lung is the transpulmonary route, but it is limited by the lung's tendency to expel materials entering through the airways and, therefore, the inability of the drug to stay in contact with the diseased tissues for an adequate amount of time.³ Moreover, the epithelial barrier of the deep lung has a high resistance (1,200 Ω -cm² higher than intestinal mucosa)⁴ and is equipped with fewer transporter and channel proteins,^{4,5} which reduces drug absorption to a great extent.

The use of nanoparticle-mediated delivery of therapeutic molecules may be promising in overcoming the obstacles in drug delivery to the lungs and enhancing drug release. Attempts have been made to use lipid, polylactide-co-glycolide, albumin, poly(ω -pentadecalactone-co-butylene-co-succinate), cerium oxide, gold, ultrasmall superparamagnetic iron oxide

nanoparticles, superparamagnetic iron oxide, lipid-polycation-DNA, *N*-[1-(2,3-dioleoyloxy)propyl]-NNN-trimethylammoniummethyl sulfate, silica-overcoated magnetic cores, and polyethyleneglycol phosphatidylethanolamine (PE) nanoparticles to deliver drugs and therapeutic genes to treat lung cancers.¹ Although several nanoparticle-mediated anticancer therapeutic systems have

¹ Center for Research and Education in Nanobioengineering, University of South Florida College of Medicine, Tampa, FL, USA

² Department of Internal Medicine, University of South Florida College of Medicine, Tampa, FL, USA

³ Department of Molecular Medicine, University of South Florida College of Medicine, Tampa, FL, USA

⁴ James A. Haley Veterans Hospital, Tampa, FL, USA

Submitted: November 21, 2016. Revised: April 18, 2017.

Accepted: April 25, 2017.

Corresponding Author:

Subhra Mohapatra, Department of Molecular Medicine, University of South Florida College of Medicine, 12901 Bruce B. Downs Blvd, Tampa, FL 33612, USA.

Email: smohapa2@health.usf.edu



reached clinical trials or received United States Food and Drug Administration (FDA) approval,⁶ delivery of these nanoparticles to the deep lung has met with little success. Recently, Howell et al. have formulated lipid micelle nanoparticles (LMNs) using FDA approved ingredients such as polyethylene glycol (PEG-2000), PE, DC-cholesterol, and dioleoyl-PE (DOPE). The core of these particles can be filled with drugs such as doxorubicin (Dox) or magnetic resonance imaging contrast agents and thus serve as an excellent drug delivery platform for theranostics in biological systems, especially the lungs.^{7,8,9,10} Dox is a widely used chemotherapeutic agent to treat lung, breast, bone, and brain cancers. However, its use is severely restricted because of its toxic side effects such as esophagitis, cardiac toxicity, and hepatotoxicity. In this study, we have shown that encapsulating Dox in LMNs reduces Dox-induced toxicity.

Overcoming the physiological rejection and immune responses against nanoparticles remains an obstacle for drug delivery to the lungs. One way to overcome this obstacle is to develop a biocompatible cell-based drug delivery system which will be able to deliver the payload to the target organ and at the same time will help in avoiding physiological and immune rejection. Owing to their immunocompetent properties, Sertoli cells (SCs) have long been used to facilitate allo- and xenogeneic cell transplantation.^{11,12} In addition, xenogeneic SCs have been found to induce donor-specific tolerance in the host when administered intravenously.¹⁰ Dufour et al. have shown immunoprotection rendered by rat SCs for islet cells during xenotransplantation without immunosuppression.^{13,14} Recently, Halley et al. used genetically engineered SCs producing insulin to treat diabetes in mice.¹⁵

Previously, we described a method to deliver curcumin to the deep lungs of normal mice using isolated rat SCs³ in asthmatic mice. Since SCs are expected to deliver drugs in the capillary bed, where a majority of metastatic tumors are found, we reasoned that SCs packed with nanodrug delivery systems carrying anticancer drugs may provide an ideal system. In this study, we delivered Dox to treat Lewis lung carcinoma 1 (LLC1)-induced lung cancer in mice. We also encapsulated Dox in lipid micellar nanoparticles (DLMN) in order to reduce its toxicity while keeping its efficacy unaltered. Then we preloaded this formulation in SCs which enabled us to deliver the drug to the deep lung where drug delivery is otherwise limited. The results of these studies demonstrate that SC-loaded DLMNs provide an effective approach to treat lung cancer with significantly reduced Dox-induced toxicity.

Materials and Methods

All animal experimental protocols used in this study were approved by the Institutional Animal Care and Use Committee of the University of South Florida, Tampa, FL, USA. Rats and mice used in the study were housed in the animal facility with food and water available ad libitum during the period of the study. Animal health was monitored daily from the study

start date until the study end date. All animals used in this study were coded and analysis of the results was performed by persons blinded to the experimental groups.

Preparation of Nanoparticles

LMNs were prepared by the method described by Howell et al.⁹ with some modifications. Briefly, Dox hydrochloride (Dox; LC Laboratories, Woburn, MA, USA) along with 4M equivalents of triethylamine was added to chloroform and the mixture was sonicated for 30 min to dissolve the Dox. Dox was encapsulated inside micelles. PEG-2000 PE (0.1 mg, 2% of total), 3 β -[N-(Dimethylaminoethane)carbamoyl]cholesterol (DC cholesterol) (7.9 μ M, 3.95 mg, 66% of total), and DOPE (2.6 μ M, 1.95 mg, 32% of total) were added to 1.5 mL of chloroform. Three milligrams of the Dox in chloroform were then added to this solution. To ensure complete solubilization, the reaction solution was sonicated in a Branson 2510 sonicator (Thermo - Fisher Scientific, Weehawken, NJ, USA) for 20 min. The solution was then left to evaporate for 2 h in a vacuum oven at 40 °C. The dry film was heated at 80 °C for 2 min. Then, 2 mL of water was added, and the solution was again sonicated. The DLMNs were then filtered through a 0.45- μ m syringe filter and subsequently dialyzed (3,000 kDa molecular weight cut off) in water overnight. Once the nanoparticles were taken off dialysis they were frozen at -80 °C for 2 h. The frozen solution was then freeze dried at 0.05 mBar overnight and stored as a powder at 4 °C until further use. The dried micelles were dissolved in water and filled with Dox at a concentration of 0.26 μ g Dox per microgram of LMN to produce DLMN.

Induction of Lung Tumors in Mice

LLC1 cells (cat # CRL-1642, ATCC, Manassus, VA, USA) were cultured with Dulbecco's modified Eagle medium (DMEM) supplemented with 10% fetal bovine serum (FBS) and 1% penicillin and streptomycin. A total of 80 C57BL/6 mice were used to induce lung tumors. To induce lung tumors, 1 million (M) LLC1 cells in sterile phosphate buffered saline (PBS) were injected intravenously (iv) through the tail vein of the mice. Mice were returned to their housing and observed throughout the period of experiments. Body weight was taken for each mouse before LLC1 injection as well as at the termination of the experiment for the surviving mice.

SC Culture, Loading, and Injection into Mice

Seventeen day old Sprague-Dawley (SD) rats were used for SC isolation. Rat pups were euthanized by carbon dioxide inhalation and testes were surgically removed, then digested sequentially with trypsin and collagenase as reported by Cameron et al. and Gloat.^{3,16,17} Cells were maintained in DMEM/F12 supplemented with insulin-transferrin-selenium (1% ITS, Invitrogen, Waltham, MA, USA) and

gentamicin sulfate (50 mg/mL, Sigma, Saint Louis, MO, USA) for at least 10 d. Upon 90% confluency, SCs were incubated with Dox (65 µg/mouse/dose), DLMNs (250 µg/mouse/dose, 65 µg do equivalent), or LMNs (250 µg/mouse/dose) for 3 h and then aggressively washed with PBS to remove molecules attached loosely on the surface of the cells; they were then resuspended in 100 µL of sterile saline for iv injection. Ten days after LLC1 injection, mice were randomly divided into 5 groups. Four million SCs per mouse were injected through iv route 10 d and 17 d after LLC1 injection. The control group (LLC1 group) did not receive any SCs. The SC group received SCs only, the SC-Dox group received SCs loaded with Dox, the SC-LMN group received SCs loaded with LMN, and the SC-DLMN group received SCs loaded with DLMN. Naive animals did not receive any LLC1 injection or any treatment at all (naive group).

Confocal Microscopy

After loading the SCs with Dox, LMN, or DLMN, confocal fluorescence microscopy was performed on live cells to capture the Dox fluorescence using Leica TCS SP2 Laser Scanning Confocal Microscope (Leica Microsystems, Buffalo Grove, IL, USA). Dox fluorescence was quantitated from the time series images using Image J software (version 1.49, National Institutes of Health [NIH], Bethesda, MD, USA).

Tissue Collection, Processing, and Histology

Mice were deeply anesthetized 24 d after LLC1 injection by ketamine and xylazine (100 mg/kg and 20 mg/kg, respectively). From the pilot experiments, this study period was determined as optimal with minimal animal suffering. Therefore, this time period was used for the current study. Body weight was taken. Blood was collected by cardiac puncture. This allowed us to maximize blood collection without distress to the animal. Serum was stored at -80 °C until used. The lungs were inflated with 200 µL of sterile PBS through the trachea, harvested and transferred to 4% paraformaldehyde (PFA) for fixation. The heart and liver were also collected and weighed immediately after extraction. The cardiac ventricles were divided into 2 parts. One part was snap frozen on dry ice and stored at -80 °C until further use. The remaining part was fixed with 4% PFA. The liver was also snap frozen or fixed with 4% PFA. After 24 h, lungs were dehydrated, infiltrated, and then embedded in paraffin wax. Five micrometer sections of the whole lung were collected on glass slides for future staining experiments. The heart and liver were infiltrated with 30% sucrose solution and embedded in optimum cutting temperature compound. Seven-micrometer thick cryosections were collected on superfrost plus slides for different staining experiments. Bright field microscopy was performed to visualize the histological changes in the tissues using

Olympus 71X microscope (Olympus corporation of the Americas, Waltham, MA, USA).

Hematoxylin and Eosin (H&E) Staining

H&E staining was performed on lung, heart, and liver sections. Lung sections were stained with H&E using an automated staining system (Leica Autostainer XL). Heart and liver sections were washed with PBS for 5 min, stained with H&E for 30 s and 1 min, respectively, and then dehydrated with graded alcohol, cleared with xylene, and coverslipped with VectaMount mounting medium (Vector Laboratories Inc., Burlingame, CA, USA).

Immunohistochemistry

Slide-mounted whole lung sections were immunostained using rabbit anti-Ki67 antibody (1:100, Spring Biosciences, Pleasanton, CA, USA) with an automated immunostaining system (Ventana Discovery XT automated system; Ventana Medical Systems, Tucson, AZ, USA). Slide-mounted heart sections were washed with PBS, heated in antigen unmasking solution (1:100; Vector Laboratories Inc., Burlingame, CA, USA) for 20 min at 90 °C, incubated in 3% hydrogen peroxide for 20 min, and washed 3 times in PBS. The sections were then incubated for 1 h in permeabilization buffer (10% goat serum, 0.1% Triton X-100 in PBS) at room temperature and incubated overnight at 4 °C with rabbit anti-Troponin I antibody (1:200). The following day, sections were washed with PBS and incubated serially with biotinylated goat anti-rabbit (1:400, Vector Laboratories Inc.) antibody in antibody solution and avidin-biotin complex mixture (1:100; Vector Laboratories Inc.) for 1 h at room temperature and visualized using 3,3'-diaminobenzidine (DAB)/peroxide substrate solution (Vector Laboratories Inc.) with PBS washes in between. After the final wash, sections were dehydrated with increasing concentrations of ethanol (70%, 95%, 100%), cleared with xylene, and coverslipped with Vectamount mounting medium.

Measurement of LLC1-Induced Tumor Burden in the Lung

Low magnification bright field images from H&E-stained lung sections were collaged and imported to Image J software. Hematoxylin staining intensity was measured from each lung section and expressed as integrated density. Ki67 immunoreactivity was also measured from the immunostained sections using Image J.

Enzyme-linked immunosorbent assay (ELISA) for Cardiac Troponin I (cTnI) Subunit Estimation

cTnI in heart tissue lysates or serum samples was measured using cTnI ELISA kit (Life Diagnostics, West Chester, PA, USA) following manufacturer's instructions. Snap frozen heart tissues were homogenized using tris-buffered saline

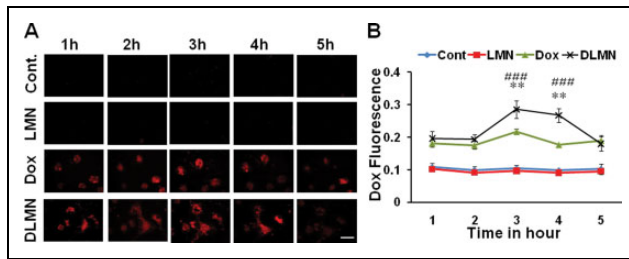


Fig. 1. Sertoli cells uptake Dox or DLMN in vitro. (A) Live confocal microscopic images showing the Dox fluorescence (red) in the Sertoli cells incubated with or without LMN, Dox, or DLMN for different time periods. Scale bar = 60 μ . (B) Image J quantification of Dox fluorescence shows maximum DLMN uptake by the cells at 3 h post incubation. $**P < 0.01$ versus Free Dox. $###P < 0.001$ versus LMN. DLMN, Dox conjugated to lipid micelle nanoparticles; LMN, lipid micelle nanoparticle; Dox, doxorubicin.

(TBS)-ethylenediaminetetraacetic acid (EDTA) buffer with protease and phosphatase inhibitors (Fisher Scientific). Sample volume was reduced to 25 μ L/well for low serum volume obtained from mice and reagent volumes were adjusted accordingly. Briefly, 25 μ L of samples were incubated in an antibody coated 96 well plate along with cTnI antibody conjugated with horse raddish peroxidase (cTnI-HRP) at room temperature for 1 h, then incubated with 25 μ L 3,3',5,5' tetramethylbenzidine (TMB, Fisher Scientific) solution for 20 min at room temperature. The reaction was stopped with 2N H₂SO₄ and read at 450 nm. A Bradford assay was performed to estimate the total protein concentrations in the samples used. cTnI concentration was expressed per milligram of total protein in the respective sample.

Measurement of Liver Enzymes

Aspartate aminotransferase (AST) activity was measured from the liver lysates using AST colorimetric assay kit from Biovision (Milpitas, CA, USA) following manufacturer's instructions. Fifty milligram of liver samples were homogenized in 200 μ L of the assay buffer. After the reaction mix containing the enzyme mix, developer and substrate were added to the samples, the plate was incubated at 37 $^{\circ}$ C. A reading was taken every 30 min for a period of 150 min. Optical density (OD) value at 450 nm at 30 min was taken as initial and at 120 min was taken as final. AST activity was expressed as milliunits per microliter.

Statistical Analyses

All data are presented as mean \pm standard error of the mean (SEM). Statistical significance was evaluated by one-way analysis of variance (ANOVA) with Bonferroni post hoc test. For the survival analysis, two-way ANOVA with Tukey's post hoc test was used for comparison. A *P* value of less than 0.05 was considered statistically significant for all comparisons.

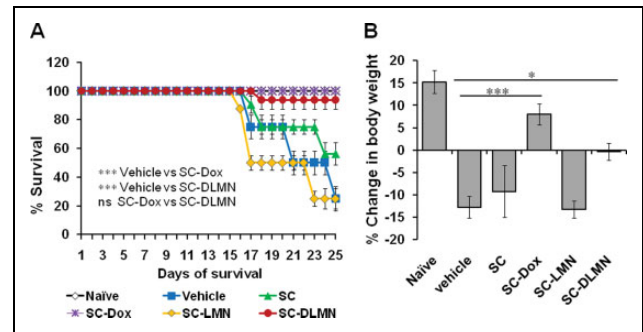


Fig. 2. SC-dox or SC-DLMN increases the survival of LLC1 injected mice and improves the body weight. (A) Kaplan–Meier survival curve showing the percentage of mice survived (% survival, mean \pm SEM) in different groups during 25-d period after LLC1 injection. (B) Histogram shows the percentage change in body weight (\pm SEM) of mice in different experimental groups after LLC1 injection. $*P < 0.05$. $***P < 0.001$, ns, not significant; SC, Sertoli cell; Dox, doxorubicin; DLMN, Dox conjugated to lipid micelle nanoparticles; LLC1, Lewis lung carcinoma 1.

Results

Uptake of Dox by SCs In Vitro

To measure Dox uptake by SCs, upon 90% confluency, SCs were incubated with Dox or DLMN. Supplementary Figure 1 shows SC culture at day 10. Combined bright field and fluorescence microscopy showed that following incubation, Dox, or DLMN entered into SCs within hours without significantly reducing the number of cells (Supplementary Fig. 2). The time-series confocal microscopy of live SCs incubated with LMN, Dox, or DLMN for 1 to 5 h showed maximum uptake of Dox or DLMN at 3 h (Fig. 1A and B) postincubation. Image J quantification of live confocal images showed maximum Dox fluorescence intensity at 3 h postincubation (Fig. 1B). These analyses also indicated that DLMNs were taken up more efficiently and retained in the cytoplasm longer than Dox (Fig. 1A). In subsequent in vivo experiments, we incubated the SCs with Dox, DLMN, or LMN for 3 h.

Effects of SC-Dox or SC-DLMN Treatments on the Survival and Body Weight of Mice Induced with Lung Tumor

To examine the efficacy of drug treatments on survival, a Kaplan–Meier survival curve (Fig. 2A) was plotted for each group of mice showing the survival of mice during the period of the experiments. Only 25% of the LLC1 mice survived until the end of the experiment. SC-Dox and SC-DLMN-treated animals showed 100% survival while 60% survival was observed in SC-treated mice. Only 25% of SC-LMN-treated mice survived the period of experiment (Fig. 2A). Body weight was taken for each mouse at the beginning and (for the surviving mice) at the end of the experiment. The naive mice gained about 15% body weight in the entire

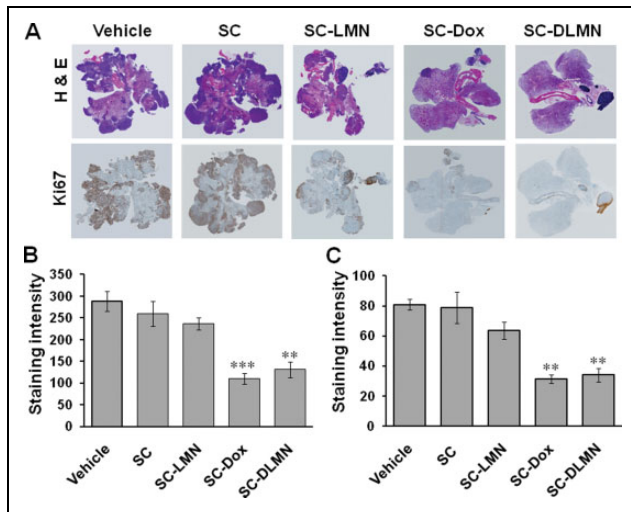


Fig. 3. SC-Dox or SC-DLMN treatment significantly decreased tumor burden in mice. (A) The upper panel shows H&E staining of lung sections under different experimental conditions. The lower panel shows the Ki67 immunostaining of the adjacent lung sections, counterstained with hematoxylin. (B) Image J analysis of H&E sections shows significant decrease in the hematoxylin staining intensity after Dox or DLMN treatment. (C) Image J analysis of Ki67 immunoreactivity. $^{***}P < 0.01$. $^{***}P < 0.001$ versus LLC1. SC, Sertoli cell; Dox, doxorubicin; DLMN, Dox conjugated to lipid micelle nanoparticles; LLC1, Lewis lung carcinoma I; H&E = hematoxylin and eosin.

period. The untreated mice bearing LLC1 lung tumors, SC-treated groups, and SC-LMN-treated groups surviving the period of the experiment lost about 10% of their body weight. On the other hand, the SC-Dox-treated mice gained weight while SC-DLMN-treated mice showed no change in body weight during the period of the experiments, thus showing significant differences from the control groups (Fig. 2B).

Effect of Drug Treatments on LLC1-Induced Lung Tumor Formation in Mice

To investigate antitumor efficacy, the effect of drug regimens on LLC1-induced lung tumor formation was examined in mice. Visual observations of untreated (LLC1), SC, or SC-LMN mice showed development of tumor nodules covering significant areas of the surface of the lungs. On the other hand, significantly less nodule formation was observed in the SC-Dox and SC-DLMN treatment groups. Histological observations of the H&E stained whole lung sections showed the spread of tumor growth inside the lungs in LLC1 injected mice as well as in the SC and SC-LMN-treated mice. In comparison to these groups, SC-Dox and SC-DLMN-treated groups of mice showed significantly reduced tumor nodule formation (Fig. 3A, upper panel). Image J quantitation further confirmed that the tumor nodules were significantly reduced in SC-Dox and SC-DLMN-treated groups (Fig. 3B). In addition to these observations, immunostaining with anti-Ki67 antibody of the lung sections

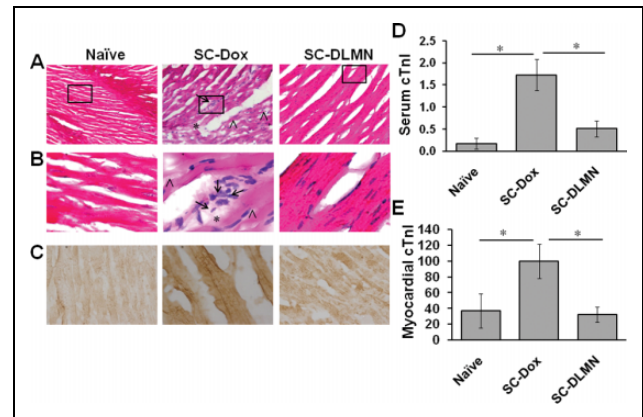


Fig. 4. DLMN protects the heart from Dox-induced toxicity. Representative bright field images of H&E staining showing tissue degeneration (*), cellular infiltration (arrow), and vacuolation (arrow head) of the left ventricular myocardium in SC-Dox or SC-DLMN-treated mice. (A) Low magnification images, scale bar = 100 μ . (B) High magnification images of the boxed areas from (A). Scale bar = 20 μ . (C) cTnI expression in the left ventricular myocardium. Scale bar = 20 μ . (D) and (E) Histograms showing elevated cTnI expression in the serum (D) or in the left ventricular myocardium (E) in SC-Dox-treated mice as determined by ELISA, $^{*}P < 0.05$. SC, Sertoli cell; Dox, doxorubicin; DLMN, Dox conjugated to lipid micelle nanoparticles; cTnI, cardiac troponin I; H&E = hematoxylin and eosin.

showed a substantially large number of Ki67-positive proliferating cells in the untreated (LLC1), SC, and SC-LMN-treated mice. Ki67 immunoreactivity was significantly reduced in mice after treatment with SC-Dox or SC-DLMN (Fig. 3A, lower panel, C). These observations indicate that SC-Dox or SC-DLMN treatments reduced the LLC1-induced tumor burden in mice. It was also observed that hematoxylin staining or Ki67 staining intensities in SC-DLMN group were not significantly different from the SC-Dox-treated group, thus indicating that the effects of SC-DLMN treatment were comparable to those of SC-Dox treatment.

DLMN Treatment Induced Less Cardiac Toxicity in Mice

Although a potent chemotherapeutic drug, Dox is highly cardiotoxic. To evaluate the cardiotoxic effect of Dox, we evaluated the cardiac tissues histologically as well as by measuring the cTnI levels of heart and serum from SC-Dox or SC-DLMN-treated mice. Histological observations of H&E-stained cardiac tissues from SC-Dox-treated mice showed signs of cardiac toxicity including increased cellular infiltration in the myocardium with significant myocardial tissue necrosis and vacuolation (Fig. 4A and B). On the other hand, the myocardium of SC-DLMN-treated mice showed significantly reduced cellular infiltration, tissue necrosis, and vacuolation (Fig. 4A and B). Immunostaining of cardiac sections with anti-cTnI antibody showed elevated cTnI

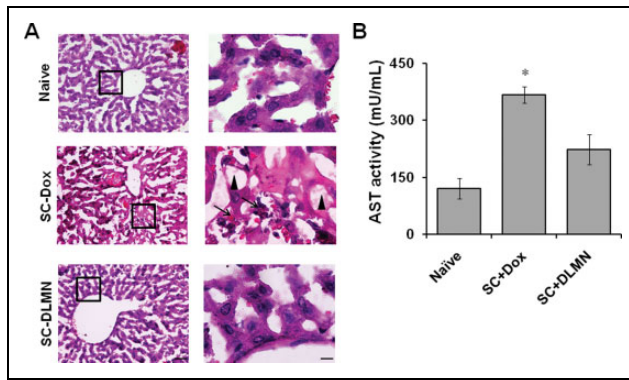


Fig. 5. DLMN protects the liver from Dox-induced toxicity in mice. (A) Representative images of H&E staining of liver sections showing the hepatic damage in SC-Dox-treated mice. Left panel shows low magnification images (scale bar = 100 μ) and right panel shows magnified images of the boxed areas in the low magnification images (scale bar = 20 μ). Vacuolation (arrow head) and hepatocellular degeneration (arrow) are evident in the SC-Dox group. (B) Histogram showing hepatic AST activity levels in naive, SC-Dox, or SC-DLMN-treated mice. * $P < 0.05$ compared to naive compared to SC-Dox. SC, Sertoli cell; Dox, doxorubicin; DLMN, Dox conjugated to lipid micelle nanoparticles; AST, aspartate aminotransferase; H&E = hematoxylin and eosin.

expression in SC-Dox-treated myocardium. Expression of cTnI in the myocardium of SC-DLMN-treated mice was reduced (Fig. 4C). Estimation of cTnI levels in the serum samples by ELISA showed elevated cTnI level in the SC-Dox treatment group indicating cardiac toxicity caused by Dox treatment in that group (Fig. 4D), subsequently confirmed by estimation of cTnI in the cardiac lysate in the same group. In both serum and cardiac lysates, cTnI levels were significantly lower in the SC-DLMN group compared to the SC-Dox treatment group (Fig. 4D, E). This observation clearly shows that SC-DLMN induced less cardiac toxicity in comparison to SC-Dox treatment in mice.

DLMN Treatment Induced Less Hepatic Toxicity in Mice

Dox is also known to cause hepatic toxicity, limiting its use in the treatment of lung cancer to a great extent. In this study, to evaluate the hepatic toxicity caused by Dox or DLMN, histological observations were performed and liver AST activities were measured in the liver homogenates of SC-Dox or SC-DLMN-treated mice. Liver sections were stained with H&E. Figure 5A shows images of the liver tissue sections from different experimental groups. The SC-Dox treatment group showed clear hepatocellular degeneration and increased cellular vacuolation and sinusoidal dilation—all indicative of hepatic toxicity. These indications were either absent or significantly reduced in the SC-DLMN-treated group (Fig. 5A). The AST assay showed increased AST activity in the liver homogenates of the SC-Dox group, indicating hepatic toxicity caused by Dox.

AST activity was significantly reduced in the SC-DLMN group compared to the SC-Dox treatment group (Fig. 5B). These observations demonstrate that DLMN is less hepatotoxic than Dox.

Discussion

A major finding of our study is that SCs can serve as a carrier of drugs and nanoparticulate drugs to the deep lung, which was probed herein using Dox, an anthracycline that has served as a powerful and widely used chemotherapeutic agent for a broad variety of solid and hematologic neoplasms. In order to achieve effective treatment outcomes in lung cancer pathologies, active compounds need optimal local delivery and assured distribution with higher penetration into the alveolar region of the lung to maximize their therapeutic effects. But current methodological limitations make drug delivery to the deep lung difficult and result in poor treatment outcome. The “nano-cell” drug delivery approach described in this report has many advantages: (1) it avoids immune rejection: cell-mediated immunity, target cell apoptosis, and complement-mediated cell lysis^{12,18}; (2) it provides immunoprotection of allo- and xenogeneic cell transplants¹³; (3) SCs (~30–50 μ m) appear to become entrapped in the precapillary vascular bed of the lung (~5 μ m) and undergo lysis to release the nanoparticulate drugs, and the lysed cells are cleared^{3,12} within 15 min from the system without deleterious effects to the individual. These properties have made SCs a great cellular carrier of therapeutic molecules. Although our observations indicate improved survival of the drug-loaded SC-treated mice in comparison to tumor bearing mice treated with free drug, at this point, the reason is not well understood and needs further investigation.

Another finding our evidence shows is that SCs are efficient in loading and delivering cytotoxic payloads such as LMN, Dox, or DLMN to the lung. Presumably, the drug was delivered when the large SCs burst in the capillary bed of the lung, releasing Dox molecules that then exerted their effects by inhibiting tumor growth. We do not have any evidence that SCs had an effect on modifying the therapeutic or safety potential of Dox or DLMN. The therapeutic efficacy of DLMN in reducing the tumor burden and increasing the survival of the mice was found to be comparable to Dox. Also, the treated mice either maintained or gained body weight. Thus, this SC-based nanodrug delivery method was able to deliver an optimal amount of drug to the lung to produce the therapeutic effects.

Dox is a potent chemotherapeutic agent and different formulations of Dox are either in clinical trials or available for therapy.¹⁹ But, as described in the literature, the clinical use of Dox is severely hampered by its adverse side effects such as shortness of breath, ankle swelling, fatigue/persistent tiredness, irregular heartbeat, myelosuppression, esophagitis, hepatotoxicity^{20–22}, and acute cardiac toxicity.^{7,8,23–27} It increases reactive oxygen species (ROS) in several organs

and damages them, with toxic effects that are cumulative and mostly irreversible. Inflammatory reactions in the veins used for injection have also been observed.²⁸ Cardiac toxicity and heart failure are common complications in patients receiving Dox chemotherapy.^{7,8,26,29} In a recent study conducted by Loncar-Turukalo et al., treatment of adult male Wistar rats for 15 d with 15 mg/kg intraperitoneal Dox caused cardiotoxicity as confirmed by histological examination. Although echocardiography showed no development of heart failure, the increase in heart rate variability reflected subtle microscopic changes in cardiac toxicity in these rats.⁷ cTnI is a useful biomarker of myocardial injury.^{25,30–32} Engle et al. described a well correlated relationship between cardiac myopathy and cTnI concentration in the serum.³⁰ In line with these observations, we have shown histological changes in the myocardium as well as increased cardiac and serum cTnI concentrations in SC-Dox-treated mice, indicating Dox-induced cardiomyopathy.

In addition to cardiac toxicity, hepatotoxicity is another serious side effect that limits the use of Dox. Singla et al. have observed that administration of Dox at a dose of 25 mg/kg for 3 d induced hepatotoxicity and oxidative stress in SD rats. They observed significant decreases in activity of catalase, superoxide dismutase, glutathione-S-transferase, glutathione peroxidase, and glutathione reductase in rat liver supernatants along with increased activity of serum glutamic pyruvic transaminase (SGPT) and serum glutamic oxaloacetic transaminase.²⁰ Dox-induced hepatic arterial and parenchymal necrosis were observed following Dox administration by Verret et al. in pigs²¹ and by Rashid et al. in rats.²² In these studies, decline in hepatic function was indicated by downregulation of genes including enzymes of lipid and carbohydrate metabolisms.²¹ Recently, increased AST and ALT activities along with histopathological changes in the liver were reported in Dox-treated rats.^{33,34} In accordance with these observations in the present study, we have observed increased hepatic AST levels in SC-Dox-treated mice associated with significant hepatic tissue damage.

In this study, we have shown that Dox-induced cardiac toxicity was significantly reduced in the SC-DLMN-treated mice. Several attempts have been made to reduce Dox-induced toxicity and improve the efficacy of Dox.^{23,35–41} Since the first FDA approval of pegylated Dox, or Doxil, in 1990, several nanotechnological formulations of the drug have entered clinical trials and shown significant pharmacologic advantages and added clinical value over Dox.^{19,23} Liposomal Dox not only improves drug penetration into tumors but also decreases drug clearance and thereby increases the duration of therapeutic drug effects. This formulation of Dox also modulates toxicity, specifically cardiotoxicity. In the present study, we conjugated Dox to LMN particles in an attempt to reduce drug-induced toxicities. In previous studies conducted by our laboratory, we observed that LMN particles were efficient in delivering drugs or genes to the lungs without any adverse

effects.^{9,10} The data from the present study support the previous observations as DLMN was comparably effective to Dox. Moreover, loading into SCs enabled the delivery of DLMN to the deepest areas of the lung, thus indicating the excellent therapeutic potential of this novel delivery method with significantly reduced cardiac and hepatic toxicity and increased clinical efficacy.

Conclusion

In conclusion, in this study, we developed a novel method to deliver chemotherapeutic drugs to treat lung cancer. Conjugating Dox with LMN particles (DLMN) significantly reduced the toxic side effects of this drug while keeping its efficacy unaltered. Preloading the formulation in immunocompetent SCs facilitated delivery of the drug to the deep lung and successful treatment of lung tumors which would otherwise be difficult to treat.

Ethical Approval

This study was approved by the Institutional Animal Care and Use Committee (IACUC) of University of South Florida, Tampa, FL, USA.

Statement of Human and Animal Rights

Rats and mice used in the study were housed in the animal facility with food and water available ad libitum during the period of the study. Animal health was monitored daily.

Statement of Informed Consent

There are no human subjects in this article and informed consent is not applicable.

Declaration of Conflicting Interests

The author(s) declared no potential conflicts of interest with respect to the research, authorship, and/or publication of this article.

Funding

The author(s) disclosed receipt of the following financial support for the research, authorship, and/or publication of this article: This research was supported by National Institute of Health Grant R01CA152005.

Supplementary Material

The supplementary figures for this article are available online.

References

1. Chandolu V, Dass CR. Treatment of lung cancer using nanoparticle drug delivery systems. *Curr Drug Discov Technol.* 2013;10(2):170–176.
2. Vogl TJ, Shafinaderi M, Zangos S, Lindemayr S, Vatankhah K. Regional chemotherapy of the lung: transpulmonary chemoembolization in malignant lung tumors. *Semin Intervent Radiol.* 2014;30(2):176–184.
3. Kumar A, Glaum M, El-Badri N, Mohapatra S, Haller E, Park S, Patrick L, Nattkemper L, Vo D, Cameron DF. Initial observations of cell-mediated drug delivery to the deep lung. *Cell Transplant.* 2010;20(5):609–618.

4. Da Silva AL, Santos RS, Xisto DG, Alonso Sdel V, Morales MM, Rocco PR. Nanoparticle-based therapy for respiratory diseases. *An Acad Bras Cienc.* 2013;85(1):137–146.
5. Bur M, Henning A, Hein S, Schneider M, Lehr CM. Inhalative nanomedicine—opportunities and challenges. *Inhal Toxicol.* 2009;21(suppl 1):137–143.
6. Iwamoto T. Clinical application of drug delivery systems in cancer chemotherapy: review of the efficacy and side effects of approved drugs. *Biol Pharm Bull.* 2013;36(5):715–718.
7. Loncar-Turukalo T, Vasic M, Tasic T, Mijatovic G, Glumac S, Bajic D, Japunzic-Zigon N. Heart rate dynamics in doxorubicin-induced cardiomyopathy. *Physiol Meas.* 2015;36(4):727–739.
8. Santacruz L, Darrabie MD, Mantilla JG, Mishra R, Feger BJ, Jacobs DO. Creatine supplementation reduces doxorubicin-induced cardiomyocellular injury. *Cardiovasc Toxicol.* 2015;15(2):180–188.
9. Howell M, Mallela J, Wang C, Ravi S, Dixit S, Garapati U, Mohapatra S. Manganese-loaded lipid-micellar theranostics for simultaneous drug and gene delivery to lungs. *J Control Release.* 2013;167(2):210–218.
10. Howell M, Wang C, Mahmood A, Hellermann G, Mohapatra SS, Mohapatra S. Dual-function theranostic nanoparticles for drug delivery and medical imaging contrast: perspectives and challenges for use in lung diseases. *Drug Deliv Transl Res.* 2013;3(4):352–363.
11. Saah M, Wu WM, Eberst K, Marvanyos E, Bodor N. Design, synthesis, and pharmacokinetic evaluation of a chemical delivery system for drug targeting to lung tissue. *J Pharm Sci.* 1996;85(5):496–504.
12. Shamekh R, El-Badri NS, Saporta S, Pascual C, Sanberg PR, Cameron DF. Sertoli cells induce systemic donor-specific tolerance in xenogenic transplantation model. *Cell Transplant.* 2006;15(1):45–53.
13. Dufour JM, Rajotte RV, Kin T, Korbitt GS. Immunoprotection of rat islet xenografts by cotransplantation with sertoli cells and a single injection of antilymphocyte serum. *Transplantation.* 2003;75(9):1594–1596.
14. Dufour JM, Rajotte RV, Seeberger K, Kin T, Korbitt GS. Long-term survival of neonatal porcine Sertoli cells in non-immunosuppressed rats. *Xenotransplantation.* 2003;10(6):577–586.
15. Halley K, Dyson EL, Kaur G, Mital P, Uong PM, Dass B, Crowell SN, Dufour JM. Delivery of a therapeutic protein by immune-privileged Sertoli cells. *Cell Transplant.* 2011;19(12):1645–1657.
16. Cameron DF, Muffly KE. Hormonal regulation of spermatid binding. *J Cell Sci.* 1991;100(pt 3):623–633.
17. Golat BT, Cameron DF. Sertoli cells enhance formation of capillary-like structures in vitro. *Cell Transplant.* 2008;17(10-11):1135–1144.
18. Emerich DF, Hemendinger R, Halberstadt CR. The testicular-derived Sertoli cell: cellular immunoscience to enable transplantation. *Cell Transplant.* 2003;12(4):335–349.
19. Cagel M, Grotz E, Bernabeu E, Moreton MA, Chiappetta DA. Doxorubicin: nanotechnological overviews from bench to bedside. *Drug Discov Today.* 2017;22(2):270–281.
20. Singla S, Kumar NR, Kaur J. In vivo studies on the protective effect of propolis on doxorubicin-induced toxicity in liver of male rats. *Toxicol Int.* 2014;21(2):191–195.
21. Verret V, Namur J, Ghegediban SH, Wassef M, Moine L, Bonneau M, Pelage JP, Laurent A. Toxicity of doxorubicin on pig liver after chemoembolization with doxorubicin-loaded microspheres: a pilot DNA-microarrays and histology study. *Cardiovasc Intervent Radiol.* 2013;36(1):204–212.
22. Rashid S, Ali N, Nafees S, Ahmad ST, Arjumand W, Hasan SK, Sultana S. Alleviation of doxorubicin-induced nephrotoxicity and hepatotoxicity by chrysin in Wistar rats. *Toxicol Mech Methods.* 2013;23(5):337–345.
23. Tahover E, Patil YP, Gabizon AA. Emerging delivery systems to reduce doxorubicin cardiotoxicity and improve therapeutic index: focus on liposomes. *Anticancer Drugs.* 2015;26(3):241–258.
24. Pecoraro M, Sorrentino R, Franceschelli S, Del Pizzo M, Pinto A, Popolo A. Doxorubicin-mediated cardiotoxicity: role of mitochondrial connexin 43. *Cardiovasc Toxicol.* 2015;15(4):366–376.
25. Nishimura Y, Kondo C, Morikawa Y, Tonomura Y, Torii M, Yamate J, Uehara T. Plasma miR-208 as a useful biomarker for drug-induced cardiotoxicity in rats. *J Appl Toxicol.* 2015;35(2):173–180.
26. Toldo S, Goehle RW, Lotrionte M, Mezzaroma E, Sumner ET, Biondi-Zoccai GG, Seropian IM, Van Tassel BW, Loperfido F, Palazzoni G, et al. Comparative cardiac toxicity of anthracyclines in vitro and in vivo in the mouse. *PLoS One.* 2013;8(3):e58421.
27. Shivakumar P, Rani MU, Reddy AG, Anjaneyulu Y. A study on the toxic effects of Doxorubicin on the histology of certain organs. *Toxicol Int.* 2012;19(3):241–244.
28. Brayfield AE. *Martindale: The Complete Drug Reference.* 2014;22:12.
29. Zhang SH, Wang WQ, Wang JL. Protective effect of tetrahydroxystilbene glucoside on cardiotoxicity induced by doxorubicin in vitro and in vivo. *Acta Pharmacol Sin.* 2009;30(11):1479–1487.
30. Engle SK, Jordan WH, Pritt ML, Chiang AY, Davis MA, Zimmermann JL, Rudmann DG, Heinz-Taheny KM, Irizarry AR, Yamamoto Y, et al. Qualification of cardiac troponin I concentration in mouse serum using isoproterenol and implementation in pharmacology studies to accelerate drug development. *Toxicol Pathol.* 2009;37(5):617–628.
31. Engle SK, Solter PF, Credille KM, Bull CM, Adams S, Berna MJ, Schultze AE, Rothstein EC, Cockman MD, Pritt ML, et al. Detection of left ventricular hypertrophy in rats administered a peroxisome proliferator-activated receptor alpha/gamma dual agonist using natriuretic peptides and imaging. *Toxicol Sci.* 2010;114(2):183–192.
32. Ricevuto E, Cocciolone V, Mancini M, Cannita K, Romano S, Bruera G, Pelliccione M, Adinolfi MI, Ciccozzi A, Bafile A, et al. Dose-dense nonpegylated liposomal Doxorubicin and docetaxel combination in breast cancer: dose-finding study. *Oncologist.* 2015;20(2):109–110.
33. Kumral A, Giris M, Soluk-Tekkesin M, Olgac V, Dogru-Abbasoglu S, Turkoglu U, Uysal M. Beneficial effects of

- carnosine and carnosine plus vitamin E treatments on doxorubicin-induced oxidative stress and cardiac, hepatic, and renal toxicity in rats. *Hum Exp Toxicol*. 2016;35(6):635–643.
34. Kumral A, Giris M, Soluk-Tekkesin M, Olgac V, Dogru-Abbasoglu S, Turkoglu U, Uysal M. Effect of olive leaf extract treatment on doxorubicin-induced cardiac, hepatic and renal toxicity in rats. *Pathophysiology*. 2015;22(2):117–123.
 35. Peng LH, Zhang YH, Han LJ, Zhang CZ, Wu JH, Wang XR, Gao JQ, Mao ZW. Cell Membrane capsules for encapsulation of chemotherapeutic and cancer cell targeting in vivo. *ACS Appl Mater Interfaces*. 2015;7(33):18628–18637.
 36. Peng M, Li H, Luo Z, Kong J, Wan Y, Zheng L, Zhang Q, Niu H, Vermorken A, Van de Ven W, et al. Dextran-coated superparamagnetic nanoparticles as potential cancer drug carriers in vivo. *Nanoscale*. 2015;7(25):11155–11162.
 37. Peng PC, Hong RL, Tsai YJ, Li PT, Tsai T, Chen CT. Dual-effect liposomes encapsulated with doxorubicin and chlorin e6 augment the therapeutic effect of tumor treatment. *Lasers Surg Med*. 2015;47(1):77–87.
 38. Wang H, Xu Y, Zhou X. Docetaxel-loaded chitosan microspheres as a lung targeted drug delivery system: in vitro and in vivo evaluation. *Int J Mol Sci*. 2014;15(3):3519–3532.
 39. Li M, Song W, Tang Z, Lv S, Lin L, Sun H, Li Q, Yang Y, Hong H, Chen X. Nanoscaled poly(L-glutamic acid)/doxorubicin-amphiphile complex as pH-responsive drug delivery system for effective treatment of nonsmall cell lung cancer. *ACS Appl Mater Interfaces*. 2013;5(5):1781–1792.
 40. Olson LE, Bedja D, Alvey SJ, Cardounel AJ, Gabrielson KL, Reeves RH. Protection from doxorubicin-induced cardiac toxicity in mice with a null allele of carbonyl reductase 1. *Cancer Res*. 2003;63(20):6602–6606.
 41. Rau KM, Lin YC, Chen YY, Chen JS, Lee KD, Wang CH, Chang HK. Pegylated liposomal doxorubicin (Lipo-Dox(R)) combined with cyclophosphamide and 5-fluorouracil is effective and safe as salvage chemotherapy in taxane-treated metastatic breast cancer: an open-label, multi-center, non-comparative phase II study. *BMC Cancer*. 2015;15:423.